CrossMark

Effect of surfactant and radiation treatment on the morphology and properties of PP/EG composites

J. S. Sefadi[1] · A. S. Luyt[1,2] · J. Pionteck[3] · U. Gohs[3]

Abstract The effects of surfactant and electron beam (EB) radiation treatment on the morphology and properties of polypropylene (PP)/expanded graphite (EG) composites were investigated. Surfactant treatment and sonication of EG before mixing with PP significantly influenced the morphologies of the composites, and the modification of EG with sodium dodecyl sulphate (SDS) had a strong negative influence on the electrical conductivities of these composites. The electrical percolation concentration is shifted from 5 to 6 wt% filler to about 10 wt% filler in the presence of SDS. The melting and crystallization temperatures of PP in the composites were not affected by surfactant or EB radiation treatment. There were small differences in PP crystallinity, depending on the type and combination of treatments. The filler particles acted as nucleating agents and the crystallization temperatures shifted to higher temperatures. The thermal stability of PP was significantly higher after irradiation, and improved even further for the samples containing EG, but the presence of EG had little influence on the thermal stabilities of the non-irradiated composites. For both non-irradiated and irradiated composites the maximum tensile stress and elongation at break values are lower than the neat matrix, while the tensile modulus increased significantly.

✉ A. S. Luyt
LuytAS@qwa.ufs.ac.za; aluyt@qu.edu.qa

1 Department of Chemistry, University of the Free State (Qwaqwa Campus), Private Bag X13, Phuthaditjhaba 9866, South Africa

2 Center for Advanced Materials, Qatar University, PO Box 2713, Doha, Qatar

3 Leibniz-Institute für Polymerforschung Dresden e.V., Hohe Str. 6, 01069 Dresden, Germany

Introduction

Isotactic polypropylene (PP) is an important and excellent structural commodity to be used as a matrix in polymer composites because of its moderately low price, ease of processing, and excellent properties [1–3]. The physical and mechanical properties of semi-crystalline thermoplastic polymers depend on the degree of crystallinity [4] and on the orientation distribution of the crystalline segments. To improve the properties of PP, much emphasis has been put on the use of carbon nanotubes (CNTs) [5–9] in PP nanocomposites, but little work has been done on PP composites containing unmodified and surfactant-modified EG, and no literature could be found on such composites exposed to electron beam radiation.

Graphite possesses a very high modulus along its plane, and has excellent electrical conductivity [10]. These useful properties, and its low cost compared to CNTs, make it a useful filler for conducting polymer composites for industrial applications. However, the key challenge is still the breaking down of the bundles of EG aggregates to achieve good dispersion in an attempt to optimize the composites' performance. For this reason, several techniques were used to fabricate nanocomposites with uniformly dispersed EG platelets in a PP matrix, such as high shear mixing, and the use of sonication and gamma or electron beam radiation treatments. Sonication is the most common approach, but severe sonication might reduce the lengths of the sheets. Non-covalent functionalization, such as the use of surfactants, has regularly been used to overcome filler entanglements as a result of Van der Waals forces [11–13]. Ion or electron beam irradiation of nanocomposites has been used to modify the morphology and properties of composites [14–17]. During treatment for medical applications, a polyolefin matrix has been exposed to a sufficient amount

🖄 Springer

of radiation to induce a significant change in the mechanical properties [17].

Nanocomposites can be prepared by different methods such as melt compounding, solution intercalation and in situ polymerization [18–25]. The results of the study on the morphological and structural characterization of PP/conductive graphite nanocomposites [26] confirm the presence of some big agglomerates and the change in surface chemistry of the PP/EG composites due to the poor interaction and incompatibility between PP and EG. The study on PP nanocomposites based on non-sonicated and sonicated CNTs and exfoliated graphene nanoplatelets (xGnPs) [19] in the presence of isopropyl alcohol shows that the samples prepared after sonication had a lower percolation threshold and higher flexural strength and modulus. In an investigation of maleated PP nanocomposites reinforced with graphite oxide it was found that there was an intercalating effect from octadecylamine (ODA) surfactant where stacks of graphite sheets were partially exfoliated [27]. When investigating the influence of exfoliated graphite and clay platelets on PP it was found that the addition of exfoliated graphite nanoplatelets (xGnP) initiated the crystallization of PP at higher temperatures, confirming that xGnP acted as a nucleating agent [4], and that increasing clay content decreased the melting temperature of the nanocomposites compared to that of pure PP [28] because of the plasticizing effect of the organoclay. Melt mixing is the most industrially compatible and common method used to prepare polymer composites, even if the mixing conditions may have a strong influence on the final properties [29]. In polymer composites, electron beam radiation may induce chain scission and/or crosslinking [14–17], and may change the crystallinity or microstructure.

In the work reported in this paper, we prepared PP/EG composites, without modification, and with SDS modification, through melt mixing. Samples from all the composites were exposed to electron beam radiation. The effects of surfactant and radiation on the microstructure and properties of the composites were investigated.

Experimental

Materials

Polypropylene HKR102 was supplied in pellet form by Sasol Polymers, Johannesburg, South Africa. It is a low-flow PP homopolymer. It is formulated with a high processing stabilization package and displays low water carry over during the extrusion process. It has an MFI (230 °C/2.16 kg) of 3.5 g/10 min (ASTM D1238-ISO 1133), T_m of 163 °C, Vicat softening point of 154 °C, and density of 0.905 g cm^{-3}. Expanded graphite (EG), SIGRAFLEX

Expandat was provided by the SGL Technologies GmbH, SGL Group. It has a conductivity of 40 S cm^{-1} (room temperature, 30 MPa, self-made 2-point conductivity tester, coupled with a DMM2000 Electrometer, Keithley Instruments), an apparent volume of $\sim$400 cm^3 g^{-1}, and a specific surface area of 39.4 m^2 g^{-1} (77.4 K, N$_2$ atmosphere, Autosorb-1, Quantachrome). The sodium lauryl sulphate known as sodium dodecyl sulphate (SDS) was supplied by Sigma-Aldrich and was used without further treatment.

Composites preparation

4 g of SDS was dissolved in 5 L deionized water in a glass beaker, and 20 g of the EG was gradually added to the solution. 500 mL suspensions were sonicated for 30 min, filtered, washed with 100 mL distilled water to remove loosely absorbed SDS and dried in a vacuum oven at 50 °C for 72 h. This modified EG (containing about 5 wt% SDS), and the as-received unmodified EG, were respectively mixed with PP through melt mixing using a Brabender Plastograph 55 mL internal mixer. The mixing was done for 20 min at 60 rpm and 176 °C. The samples were compression moulded at 176 °C and 40 bar for 1 min into 1-mm-thick sheets using a LaboPress 200 T. Neat PP, as control sample, was given the same treatment in the absence and presence of SDS. The thermogravimetric analysis of the PP mixed with SDS did not show any mass loss as a result of the presence of SDS, and this sample showed exactly the same mechanical properties as the neat PP.

The PP, PP/EG, and PP/SDS-EG composites were packed in PP bags filled with nitrogen and exposed to electron beam (EB) radiation at room temperature (25 ± 1 °C). Irradiation was carried out by exposing both surfaces of the samples for uniformity. Details of the conditions and parameters employed during radiation are as follows: energy—1.5 MeV; current—4.00 mA; dose—50 kGy; distance from sample—20 cm; pulse repetition rate—75 Hz; operation frequency—1.2 kHz.

Methods

Scanning electron microscopy (SEM) analyses were carried out in a TESCAN VEGA3 Superscan scanning electron microscope (Brno, Czech Republic). The fracture surfaces of the samples were coated with gold by a Cressington Sputter Coater for 30 s. Microscope settings of 285.5 nm probe size, 50 mA probe current, 0.1 nm lateral resolution, and 30 kV AC voltage were used.

The molar mass of the PP in the different samples was determined by gel permeation chromatography (PL-GPC220 of Polymer Laboratories, RI-Detector) using two PL-MIXED-B-LS columns. The polymer was dissolved in

1,2,4-trichlorobenzene at 150 °C and 1.0 mL min^{-1} flow rate, followed by filtration. The calibrations were done with PP standards.

DSC analyses were carried out under nitrogen flow (20 mL min^{-1}) using a Perkin Elmer Pyris-1 differential scanning calorimeter (Waltham, Massachusetts, USA). The instrument was calibrated using the onset temperatures of melting of indium and zinc standards, as well as the melting enthalpy of indium. The sample masses were in the range of 5–10 mg, and they were heated from 25 to 180 °C at a heating rate of 10 °C min^{-1}. The cooling and second heating were performed under the same conditions. For all the samples, the onset and peak temperatures of melting and crystallization, as well as the melting and crystallization enthalpies, were determined from the second heating scan. The normalized enthalpies of melting and crystallization were determined according to Eqs. 1 and 2.

$$\Delta H_{\mathrm{m}}^{\mathrm{Norm}} = \frac{\Delta H_{\mathrm{m,PP}}}{w_{\mathrm{PP}}}, \tag{1}$$

where $\Delta H_{\mathrm{m,PP}}$ is the experimentally observed melting enthalpy for the PP in the composite, and $\Delta H_{\mathrm{m}}^{\mathrm{Norm}}$ is the calculated normalized enthalpy of melting for the PP weight fraction w_{PP} in the nanocomposite. The degree of crystallinity χ_{c} was calculated according to

$$\chi_{\mathrm{c}} = (\Delta H_{\mathrm{m}}^{\mathrm{Norm}}/\Delta H_{\mathrm{m}}^{\circ}) \times 100~\%, \tag{2}$$

where $\Delta H_{\mathrm{m}}^{\circ}$ is the specific enthalpy of melting for 100 % crystalline PP. A value of 209 J g^{-1} was used in the calculations [24, 25, 30].

The structures of PP and its nanocomposites filled with EG and SDS modified EG were determined through XRD. A D8 Advance diffractometer (BRUKER AXS, Germany) with PSD Vantec-1 detectors and Cu-K$_\alpha$ radiation ($\lambda = 1.5406$ Å), a tube voltage of 40 kV, a current of 40 mA and a V20 variable slit was used. The samples were scanned in locked coupled mode with 2θ ranging from 0 to 120° at 2θ increments of 0.5 s step^{-1}.

The volume resistance measurements of PP and its composites before and after radiation were carried out on a Keithley Instruments 6157A electrometer, connected to an 8009 Keithley resistivity test fixture with two plate electrodes located on the two sides of the samples. This method is appropriate for resistance values in the range from 10^7 to 10^{18} Ω at room temperature in accordance with ASTM D257-07. The corresponding conductivity values are in the range from 10^{-19} to 10^{-8} S cm^{-1}, but sensible results can be found in the range from 10^{-19} to 10^{-4} S cm^{-1}.

Thermogravimetric analysis (TGA) was done under flowing nitrogen (20 mL min^{-1}) using a Perkin Elmer TGA7 thermogravimetric analyser (Waltham, Massachusetts, USA). The samples, weighing $\pm$ 20 mg each, were heated from 30 to 600 °C at a heating rate of 10 °C min^{-1}.

The tensile properties were investigated using a Hounsfield H5KS tensile tester at a cross-head speed of 10 mm min^{-1} and a gauge length of 20 mm. All the reported values from the stress–strain curves are averages of at least five measurements for each composition.

Results and discussion

Scanning electron microscopy (SEM)

Figure 1 shows the SEM micrographs of PP/EG and PP/SDS-EG composites with and without radiation treatment. It can be seen in Fig. 1 that the dispersion of EG is inhomogeneous and the interfacial adhesion between the PP matrix and the EG sheets is weak, since big agglomerates or voids (Points A and B) are observed. The surfaces of these composites in the presence of EB irradiation seem to be slightly different, showing some cracks or detachments between the PP and the graphite sheets (Points B and D). The SDS-EG particles were fairly well dispersed in the polymer, but some areas show long agglomerated particles (Fig. 1d) indicating that the SDS treatment and sonication did not completely break up the agglomerates. Therefore, the interparticle attraction was not completely eliminated, although it seems to have been sufficiently reduced to obtain better dispersed EG particles in the PP matrix. It was not expected that the electron beam irradiation would affect the morphology or fracture surface of the samples, since the polymer did not melt during irradiation and therefore there could not have been any redispersion of the EG.

Influence of filler and radiation treatment on polymer molar mass

The number- and weight-average molar masses, as well as the dispersity indices, of pure PP and the PP/EG and PP/SDS-EG composites with and without radiation treatment were determined through gel permeation chromatography (GPC), and the results are summarized in Tables 1 and 2. The molar mass of PP in the irradiated PP/EG and PP/SDS-EG composites was lower than that of PP in the non-irradiated composites. This confirms the degradation effect of the irradiation on the PP, and it seems as if the presence of EG and SDS-EG particles did not inhibit this effect. There was an increase in number-average molar mass with increasing EG content for the irradiated samples (Table 2), which indicates the formation of a low level of radiation-induced crosslinks. This was not observed for neat PP, probably because the EG particles assisted in effectively distributing the thermal energy from the radiation. The SDS-EG samples did not show the same increase in molar mass, probably because SDS formed an isolating layer

Fig. 1 SEM micrographs of PP/expanded graphite composites: **a** 98/2 w/w PP/EG; **b** 50 kGy 98/2 w/w PP/EG; **c** 98/2 w/w PP/SDS-EG; **d** 50 kGy 98/2 w/w PP/SDS-EG
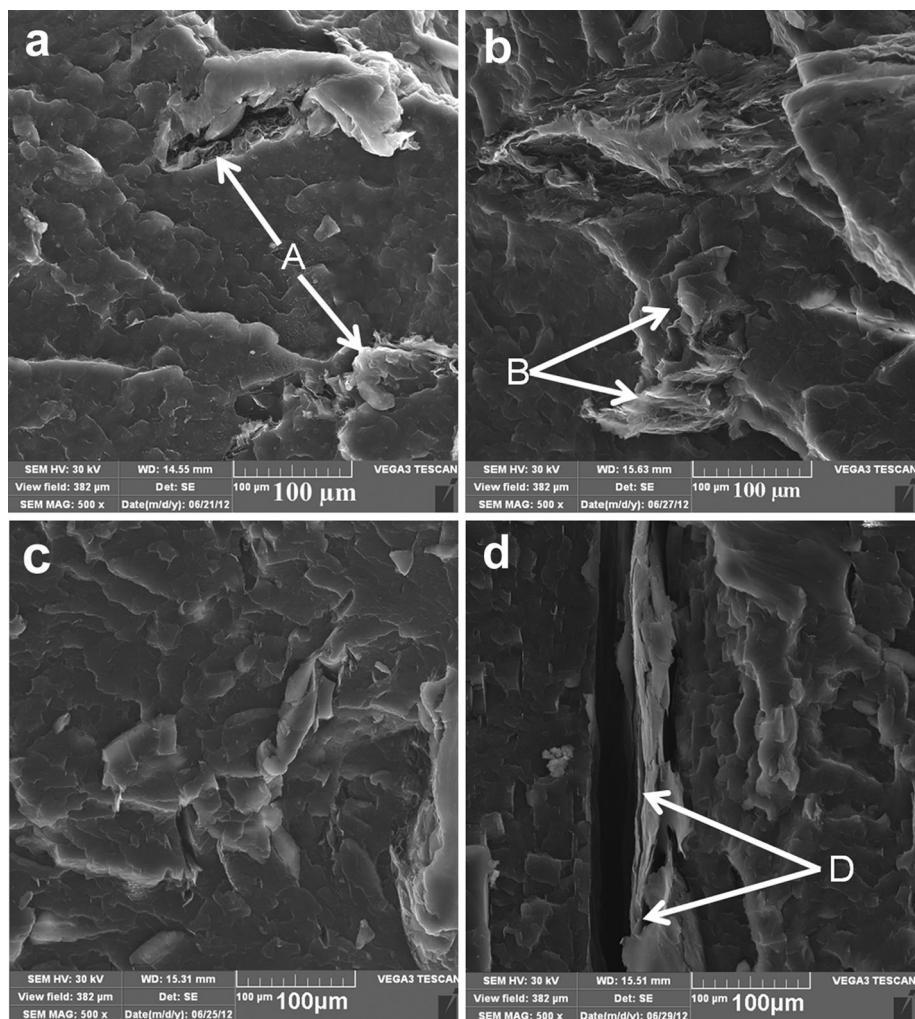
Table 1 Number-average and weight-average molar masses of the non-irradiated samples

Sample composition	M_n/g mol^{-1}	M_w/g mol^{-1}	DI (M_w/M_n)
PP	41400 ± 140	251500 ± 1410	6.1 ± 0.0
98/2 w/w PP/EG	42000 ± 990	257650 ± 210	6.1 ± 0.1
90/10 w/w PP/EG	35950 ± 1340	173900 ± 570	4.8 ± 0.2
98/2 w/w PP/SDS-EG	42200 ± 1700	257800 ± 4100	6.1 ± 0.4
90/10 w/w PP/SDS-EG	46200 ± 1840	269300 ± 140	5.8 ± 0.2

M_n number-average molar mass, M_w weight-average molar mass, *DI* dispersity index

Table 2 Number-average and weight-average molar masses of the irradiated samples
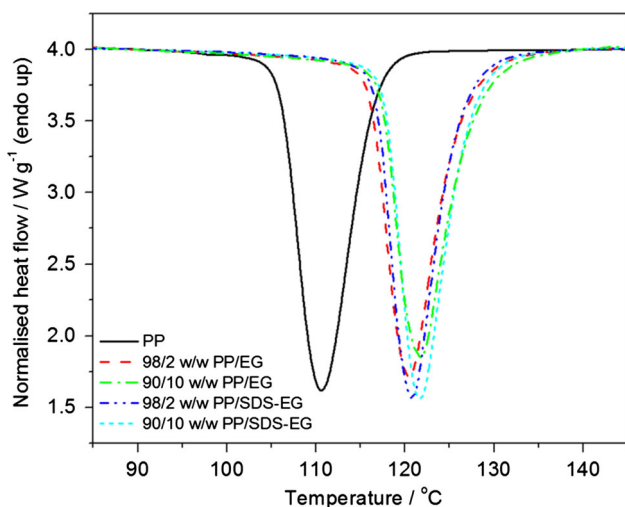
Sample composition	M_n/g mol^{-1}	M_w/g mol^{-1}	DI (M_w/M_n)
PP	33600 ± 0	255900 ± 850	7.6 ± 0.0
98/2 w/w PP/EG	35500 ± 1270	181950 ± 350	5.1 ± 0.2
90/10 w/w PP/EG	43450 ± 500	269300 ± 2550	6.2 ± 0.0
98/2 w/w PP/SDS-EG	35600 ± 280	173200 ± 2830	4.9 ± 0.1
90/10 w/w PP/SDS-EG	34750 ± 640	166950 ± 780	4.8 ± 0.1

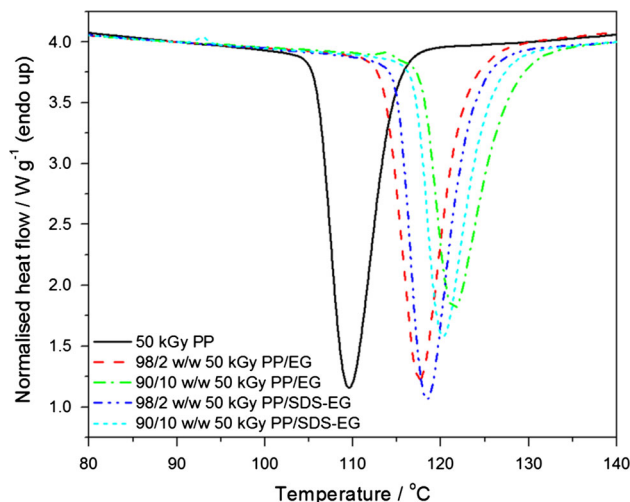M_n number-average molar mass, M_w weight-average molar mass, *DI* dispersity index

around the EG particles and prevented their effective conduction of thermal energy. The presence of SDS had a similar effect on the electrical conductivity, as can be seen from the results discussed later on in this paper. There was a visible colour change in the solvent, and the EG particles were clearly visible. There was no gel after the Soxhlet extraction, confirming that the formation of crosslinked material is a minor process during irradiation.

Differential scanning calorimetry (DSC)

The DSC cooling curves of all the investigated samples are shown in Figs. 2 and 3. The crystallization temperature of PP in all the composites is about 10 °C higher than that of neat PP (Fig. 2). The expanded graphite clearly acted as a nucleating agent for the crystallization of PP. The crystallization temperatures for the samples containing SDS-EG were the same as those of the EG containing samples within experimental error. From these results alone it seems as if the SDS modification did not significantly change the nucleation effect of the EG platelets, probably because they were not small enough and well enough dispersed despite the SDS and sonication treatment. However, the crystallinity values for the SDS-EG containing samples given in Tables 3 and 4 show that SDS treatment of EG did cause them to induce higher PP crystallinities. Although the molar masses of the irradiated samples were mostly lower than those of the non-irradiated samples, this decrease was not significant in influencing the melting temperature (Table 4). Kalaitzidou [4] and Zhang [28], who studied the influence of exfoliated graphite and clay platelets on PP, also observed that the addition of exfoliated graphite nanoplatelets initiated the crystallization of PP at higher temperatures because they acted as

Fig. 3 DSC cooling curves of irradiated PP and its irradiated composites

nucleating agents, while increasing clay contents decreased the melting temperature of the nanocomposites due to the plasticizing effect of the organoclay.

X-ray diffraction (XRD)

The XRD spectra of neat and irradiated PP, with the corresponding crystallographic planes indicated, are shown in Fig. 4. It is clear that both the neat and irradiated PP contain mostly α- or monoclinic crystals, as can be seen from the data in Table 5. There are, however, also some β- or hexagonal crystals as can be observed from the peaks at $2\theta = 16.10°$ and $21.14°$. These β-hexagonal crystal forms are attributed to many factors including (i) the presence of shearing forces during mixing, (ii) β-nucleating agents, and (iii) temperature gradients. In this study the presence of shear forces during mixing seems to be the most probable factor which induced some β-crystals in the polymer melt. The β-peak at about $2\theta = 16.10°$ is much more intense for the irradiated PP than the non-irradiated PP. The relative β-crystal content can be calculated using Eq. 3 [31].

$$k_\beta = \frac{I_\beta(300)}{[I_\alpha(110) + I_\alpha(040) + I_\alpha(130) + I_\beta(300)]} \times 100 \%,$$
(3)

where $I_\alpha(110)$, $I_\alpha(040)$, $I_\alpha(130)$, and $I_\beta(300)$ are the diffraction peak intensities of the (110), (040), (130) crystal planes of the α-crystals and the (300) crystal plane of the β-crystals. The relative β-crystal content has been calculated as 15.4 % for the non-irradiated PP and 30.6 % for the irradiated PP. According to a computer simulation study of the crystal structures of the α- and β-forms of isotactic PP [31], the α-form has alternating rows of right-handed and left-handed helices arranged into a monoclinic crystal

Fig. 2 DSC cooling curves of non-irradiated PP and its non-irradiated composites

Table 3 Melting and crystallization temperatures, melting enthalpies, and degrees of crystallinity of non-irradiated samples from the first heating and cooling DSC curves

Wt% EG	T_m/°C	T_c/°C	ΔH_m/J g^{-1}	ΔH_m^{Norm}/J g^{-1}	χ_c/%
Untreated EG					
0	164.0 ± 0.4	110.0 ± 0.1	63.9 ± 5.2	63.9	30.6
2	162.1 ± 0.3	119.9 ± 0.0	71.2 ± 3.6	72.7	34.8
4	162.8 ± 0.3	119.9 ± 0.4	69.7 ± 0.3	72.6	34.7
6	162.8 ± 0.3	119.9 ± 0.2	70.5 ± 1.7	75.0	35.9
8	162.4 ± 0.2	120.9 ± 0.3	67.0 ± 3.1	72.8	34.8
10	160.4 ± 1.8	121.9 ± 0.6	62.4 ± 0.2	69.3	33.2
SDS-treated EG					
2	162.9 ± 0.2	120.9 ± 0.8	77.1 ± 7.0	78.7	37.7
4	162.9 ± 0.5	120.9 ± 0.3	77.3 ± 3.2	80.5	38.5
6	162.4 ± 0.3	121.9 ± 0.0	70.6 ± 0.9	75.1	35.9
8	162.0 ± 0.1	120.9 ± 0.1	71.7 ± 1.8	77.9	37.3
10	162.0 ± 0.2	121.9 ± 0.6	71.3 ± 4.4	79.2	37.9

T_m melting temperature, T_c crystallization temperature, ΔH_m melting enthalpy, ΔH_m^{Norm} normalized melting enthalpy, χ_c percentage of crystallinity

Table 4 Melting and crystallization temperatures, melting enthalpies, and degrees of crystallinity of irradiated samples from the first heating and cooling DSC curves

Wt% EG	T_m/°C	T_c/°C	ΔH_m/J g^{-1}	ΔH_m^{Norm}/J g^{-1}	χ_c/%
Untreated EG					
0	162.2 ± 3.2	110.0 ± 0.2	72.2 ± 2.1	72.2	34.5
2	161.4 ± 2.1	117.9 ± 0.1	72.8 ± 4.7	74.3	35.6
4	161.0 ± 0.4	119.9 ± 0.0	68.7 ± 1.1	71.6	34.3
6	160.8 ± 0.5	119.9 ± 0.2	68.2 ± 3.2	72.6	34.7
8	160.5 ± 0.2	119.9 ± 0.3	62.4 ± 0.6	67.8	32.4
10	157.0 ± 0.6	120.9 ± 0.3	65.2 ± 6.9	72.4	34.6
SDS-treated EG					
2	161.2 ± 0.2	118.9 ± 0.2	70.7 ± 4.5	72.1	34.5
4	157.6 ± 1.2	119.9 ± 0.1	69.8 ± 3.1	72.7	34.8
6	156.9 ± 0.1	119.9 ± 0.2	72.0 ± 2.4	75.1	35.9
8	156.6 ± 0.3	119.9 ± 0.2	71.8 ± 3.3	78.0	37.3
10	160.9 ± 0.2	119.9 ± 0.3	70.6 ± 5.4	78.4	37.5

T_m melting temperature, T_c crystallization temperature, ΔH_m melting enthalpy, ΔH_m^{Norm} normalized melting enthalpy, χ_c percentage of crystallinity

structure. This is a metastable state which will not readily change into the hexagonal β-form, in which the chains form chiral domains surrounded by boundaries parallel to the (110) and (100) planes. However, it seems as if chain scission induced by EB irradiation created an environment in which the (shorter) chains could more readily rearrange into a hexagonal metastable crystal state, probably because of transformations due to localized melting during irradiation.

Figure 5 shows the XRD spectra of PP and its non-irradiated and irradiated composites filled with EG and SDS-EG. The peaks at $2\theta = 16.1°$ and $21.1°$ become weaker and eventually disappear with the introduction of EG and SDS-EG. This implies that the presence of EG and SDS-EG promoted the formation of α-crystals in PP, with a clear

reduction in the amount of β-crystals. It is, however, interesting that there was formation of some β-crystals during EB irradiation, as can be seen in the reappearance of the (300) peak at 16.1° for the irradiated samples. The EG and SDS-EG particles clearly inhibit β-crystallization of PP because of the interaction between PP and EG or SDS-EG which reduces the PP–PP interaction responsible for β-crystal formation. The peak at $2\theta = 26.6°$ is clearly related to the EG in the sample. This peak matches the crystallographic (002) plane of expanded graphite [Joint Committee on Powder Diffractions Standards JCPDS database of the International Centre for Diffraction (JCPDS 01-0646, www.icdd.com)]. There are, however, significant differences in peak intensity of the EG diffraction peak at 26.6° as a result of SDS modification and electron beam irradiation, but no
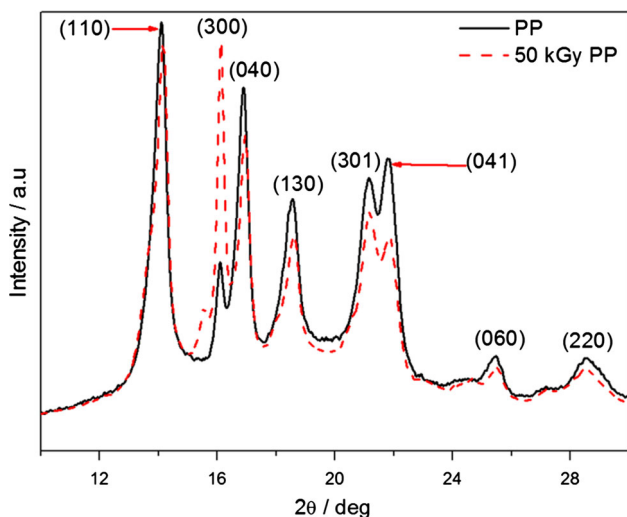
Fig. 4 XRD spectra of neat PP and irradiated PP
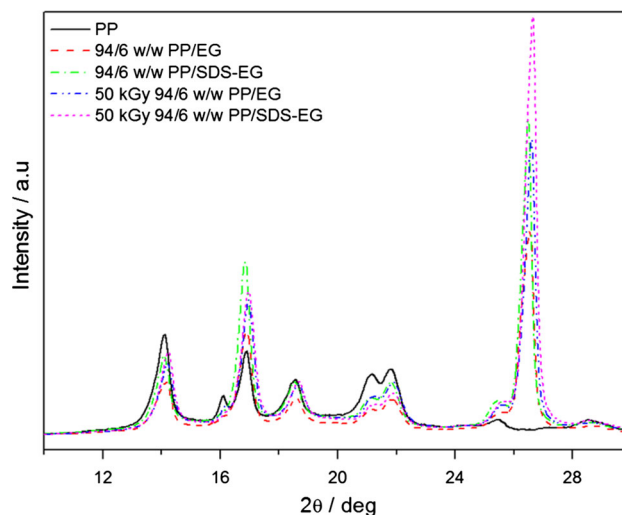
Fig. 5 XRD spectra of the non-irradiated and irradiated PP/EG and PP/SDS-EG composites

Table 5 Typical XRD peaks and intensities of neat PP with corresponding crystallographic planes

2θ	α-form	β-form	Peak intensities for non-irradiated PP	Peak intensities for irradiated PP
14.1	(110)	–	1.97×10^4	1.86×10^4
16.1	–	(300)	8.71×10^3	1.89×10^4
16.9	(040)	–	1.67×10^4	1.45×10^4
18.6	(130)	–	1.15×10^4	9.83×10^3
21.1	–	(301)	1.25×10^4	1.10×10^4
21.9	(041)	–	1.34×10^4	9.75×10^3
25.4	(060)	–	4.26×10^3	3.81×10^3
28.5	(220)	–	4.25×10^3	3.77×10^3

significant change in the peak position. This is because SDS treatment reduced the EG agglomeration, and the smaller the EG particles, the more evident was their crystal structure when analysed with XRD. It is also possible that the EB irradiation to some extent separated the EG, maybe through degradation of the polymer and penetration of the shorter chain segments into the EG agglomerates through some localized melting, which should also contribute to making the EG crystal structure more evident.

Electrical conductivity

The electrical conductivity of PP is 3.5×10^{-18} S cm^{-1}, confirming that it is an insulator. The non-irradiated and irradiated PP/EG composites exhibit a sharp transition from insulator to conductor with an electrical percolation threshold of ca. 6 and 4 wt%, respectively (Fig. 6). The difference in the percolation threshold can be attributed to defects or degradation products induced by the radiation, which created more conductive networks. The electrical
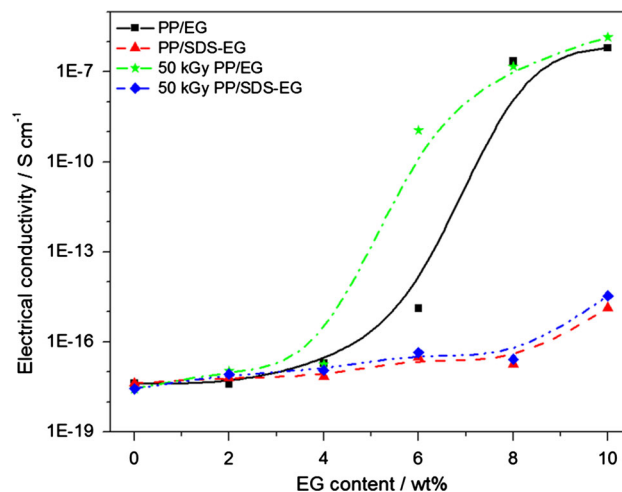
Fig. 6 Electrical conductivities of all the investigated samples

conductivity values are about the same for the non-irradiated and irradiated PP/EG composites below and above the percolation threshold. In the SDS-EG containing samples there was little increase in electrical conductivity with increasing filler content, without reaching the percolation concentration, up to the filler levels investigated in this project. Possible reasons for this observation are that (i) the presence of SDS separates the EG platelets so effectively that percolation pathways will only be formed at much higher SDS-EG contents, and (ii) the SDS forms an isolating layer around the EG platelets which reduces their effective electrical conductivity. Another study on PP nanocomposites containing CNTs and xGnP, non-sonicated and sonicated in the presence of isopropanol, showed that the samples prepared after sonication had a lower percolation

threshold of about 5 vol% compared to the 7 vol% for the samples prepared with non-sonicated filler. The reason given was that the sonication broke down the xGnP agglomerates and allowed for the formation of a continuous conductive network at lower loadings. It was, however, found that as the graphite concentration increased, the platelets can reagglomerate. The isopropanol obviously did not have the same negative effect as the SDS in our case.

Thermogravimetric analysis (TGA)

The TGA curves in Fig. 7 show a single degradation step for PP in all the samples. There is almost no difference between the temperature at 50 % mass loss for the non-irradiated samples containing up to 6 wt% EG, but this temperature increased quite significantly for the samples with higher EG contents (Table 6). There are two possible reasons for this observation: (1) The EG absorbs most of the thermal energy, so that enough energy to initiate degradation is only available at higher temperatures, and/or (2) the more agglomerated EG more effectively interacts with the volatile degradation products, which retards their diffusion out of the sample and gives rise to an observed mass loss only at higher temperatures. The temperatures at 50 % mass loss for the irradiated samples in Table 6 are scattered and show no trend with increasing EG and SDS-EG contents. This temperature is much higher for the irradiated PP than for the non-irradiated PP. The irradiation is expected to cause a fair amount of branching or weak crosslinking, and more bonds have to be broken to form volatile degradation products.

Table 6 summarizes the degradation temperatures at 50 % mass loss of the investigated samples. The PP seems to be more thermally stable after irradiation, and its stability further increases when EG is present in the case of
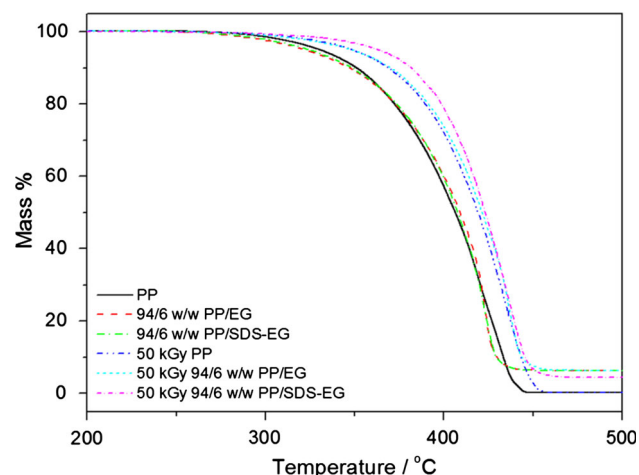
Table 6 Degradation temperatures of all the investigated samples

Wt% EG	$T_{50\%}$/°C	Wt% residue	$T_{50\%}$/°C	Wt% residue
	Non-irradiated samples		Irradiated samples	
Untreated EG				
PP	406.8	0	419.0	0
2	406.9	1.3	415.3	1.9
4	407.5	3.6	428.9	3.9
6	408.8	5.4	421.4	5.7
8	422.9	7.4	425.5	7.2
10	427.9	9.6	388.8	7.5
SDS-treated EG				
PP	406.8	0	419.0	0
2	405.7	1.5	407.5	1.0
4	407.1	3.6	415.6	3.2
6	407.4	4.0	423.3	3.8
8	417.3	4.4	416.7	5.7
10	425.7	5.8	410.2	9.9

$T_{50\%}$ is the temperature at 50 % mass loss rate

the irradiated samples, but not in the case of non-irradiated samples. The scattered results for the irradiated EG and SDS-EG containing samples could be the result of crosslinking and degradation taking place in these samples during EB irradiation. These processes probably depend upon the EG particle sizes and dispersion, which may not be consistent from one sample to the other, and therefore the degradation and mass loss processes do not occur in a consistent manner. There was no residue after the thermal degradation of non-irradiated and irradiated PP. The results in Table 6 show that there are generally very good correlations between the % residue and the amount of EG used to prepare the PP/EG samples. However, the values are generally lower for the PP/SDS-EG samples, with the exception of the irradiated sample containing 10 wt% SDS-EG, because the SDS also degrades/evaporates at temperatures below 500 °C [32].

Tensile properties

The pure PP shows typical ductile deformation behaviour with a clear yield point followed by strain softening. The presence of 6 wt% filler leads to quasi-brittle fracture during neck formation in the non-irradiated composites, while true brittle fracture was observed for the irradiated PP and its composites (Fig. 8) because of crosslinking and chain scission induced by the irradiation.

The tensile properties of all the investigated samples are summarized in Tables 7 and 8. The maximum tensile stress of the PP/EG composites generally decreased with increasing EG content. This is the result of poor wettability

Fig. 7 TGA curves of the non-irradiated and irradiated samples
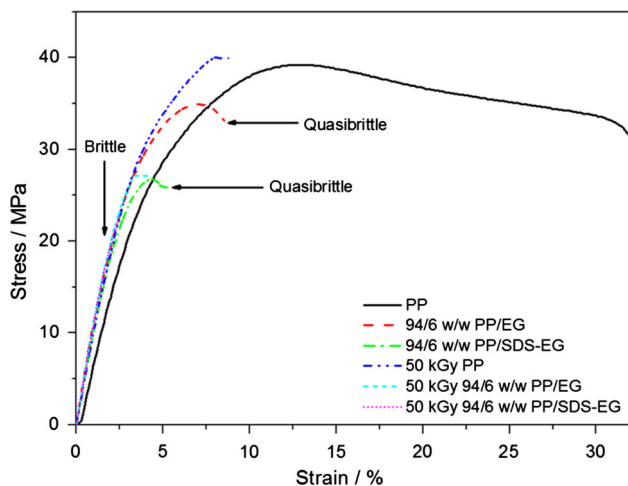
Fig. 8 Stress–strain curves of some selected samples

of the graphite by the PP and poor interfacial adhesion, which reduced the effective stress transfer across the matrix-filler interface. The EG particles then form stress concentration points at which cracks are initiated leading to stress or catastrophic failure. Although there is a slight improvement in the dispersion of SDS-EG in the PP, the maximum stress values were very similar to those of the corresponding PP/EG composites. EB irradiation did not significantly change the maximum stress values, probably because it gave rise to crosslinking and degradation, and

these two effects balanced out to such an extent that the irradiated samples show maximum stress values similar to those of the comparable non-irradiated samples.

The elongation at break decreased significantly with an increase in both EG and SDS-EG contents in the case of the non-irradiated composites. The same explanation used in the previous paragraph is also relevant here. The elongation at break of the irradiated PP/EG and PP/SDS-EG composites were lower than those of the irradiated PP, but the values did not really decrease further with increasing filler content. The lower values are the result of stress concentration at the filler particles, but since the values are already very low, the amount of filler had little influence on these values. When comparing the values in Tables 7 and 8 it can be seen that the non-irradiated PP showed significantly higher elongation at break than the irradiated PP. Irradiation initiates both crosslinking and degradation—crosslinking causes a reduction in chain mobility while degradation reduces the number of chain entanglements, both of which will give rise to lower elongation at break values.

The tensile modulus of the non-irradiated composites increased significantly with increasing EG content, but not so much with increasing SDS-EG content. An 85 % increase in tensile modulus was observed for the EG-based composites, while the increase was 28 % in the case of the SDS-EG-based samples. This is the result of the inherent

Table 7 Tensile properties of the non-irradiated samples

Untreated EG				SDS-treated EG		
Sample	$\sigma_m \pm s\sigma_m$/MPa	$\varepsilon_b \pm s\varepsilon_b$/%	$E \pm sE$/MPa	$\sigma_m \pm s\sigma_m$/MPa	$\varepsilon_b \pm s\varepsilon_b$/%	$E \pm sE$/MPa
PP	38.1 ± 0.8	26.1 ± 5.4	807 ± 26	38.1 ± 0.8	26.1 ± 5.4	807 ± 26
PP + 2 % EG	33.2 ± 0.5	9.2 ± 1.2	901 ± 105	32.1 ± 4.6	6.5 ± 1.9	1031 ± 60
PP + 4 % EG	28.5 ± 5.0	5.6 ± 0.7	1031 ± 154	31.9 ± 0.5	7.5 ± 1.7	1018 ± 119
PP + 6 % EG	31.8 ± 4.3	6.2 ± 2.1	1169 ± 65	23.9 ± 2.2	4.2 ± 0.4	999 ± 94
PP + 8 % EG	23.2 ± 4.8	4.2 ± 0.7	1169 ± 73	25.8 ± 4.0	5.5 ± 1.0	983 ± 98
PP + 10 % EG	29.8 ± 5.6	4.6 ± 1.3	1493 ± 97	23.1 ± 3.4	5.2 ± 0.8	997 ± 157

σ_m maximum stress, ε_b elongation at break, E tensile modulus, s standard deviation

Table 8 Tensile properties of the irradiated samples

Untreated EG				SDS-treated EG		
Sample	$\sigma_m \pm s\sigma_m$/MPa	Sample	$\sigma_m \pm s\sigma_m$/MPa	Sample	$\sigma_m \pm s\sigma_m$/MPa	Sample
PP	39.5 ± 3.0	9.9 ± 1.5	825 ± 167	39.5 ± 3.0	9.9 ± 1.5	825 ± 167
PP + 2 % EG	20.1 ± 2.4	2.8 ± 0.4	903 ± 101	28.3 ± 6.2	5.0 ± 1.0	965 ± 87
PP + 4 % EG	26.0 ± 0.8	4.2 ± 0.8	957 ± 219	25.9 ± 2.6	4.4 ± 1.4	836 ± 157
PP + 6 % EG	23.6 ± 4.6	3.4 ± 0.9	1091 ± 197	23.1 ± 1.7	2.9 ± 0.5	1100 ± 62
PP + 8 % EG	27.3 ± 3.1	3.5 ± 0.5	1150 ± 154	23.5 ± 7.1	3.7 ± 1.3	1031 ± 102
PP + 10 % EG	23.2 ± 1.7	3.3 ± 0.9	1202 ± 397	18.3 ± 7.5	2.5 ± 1.3	1129 ± 117

σ_m maximum stress, εb elongation at break, E tensile modulus, s standard deviation

stiffness of the EG platelets, and the interaction between PP and EG which restricted the PP segmental mobility. It is well known that stiff inorganic fillers will increase the modulus of polymer composites [33, 34]. The SDS-EG containing samples have lower modulus values than the corresponding EG composites. The reason for this is the smooth SDS layer around the EG platelets, which reduced the interaction between EG and the PP chains thereby increasing their mobility. The tensile moduli of the irradiated PP/EG and PP/SDS-EG composites were very similar to those of the comparable non-irradiated PP samples. This is an indication that the crosslinking induced by the EB irradiation was not significant enough to have an appreciable influence on the stiffness of the composites.

The research by Kalaitzidon et al. [19] showed that the samples containing sonicated xGnPs had 8 % higher strength at 3 and 10 vol% filler contents, and a 60 % higher modulus at a loading of 10 vol% compared to the samples containing non-sonicated filler. This was attributed to a better dispersion as a result of the sonication processing of the filler. In our case the sonication in SDS made little difference to the strength and modulus of the samples. EB radiation treatment (which was not previously investigated for similar systems) also had little influence on the strength and modulus of the samples.

Conclusions

The influence of anionic surfactant and EB irradiation treatment on the morphology and properties of PP/EG nanocomposites was investigated in this study. The dispersion of EG was not uniform and the interfacial adhesion between the PP matrix and the EG sheets was poor giving rise to big agglomerates. SDS treatment combined with sonication reduced the interparticle attraction and improved the dispersion of the EG particles in the polymer matrix. There were not any observable changes in the morphologies after EB irradiation. The molecular weights of the irradiated samples were generally lower than those of the non-irradiated samples, confirming that chain scission inter alia occurred as a result of irradiation. The presence of EG and SDS-EG in PP did not change the melting temperature of PP, but the filler particles acted as nucleating agents and the crystallization temperatures shifted to higher temperatures. This effect was more significant for the samples containing SDS-EG because of the better dispersion of these particles. The presence of EB irradiation had little influence on the melting temperatures. Pure PP contained both α- and β-crystals; the presence of EG and SDS-EG particles inhibited β-nucleation of the PP. Both non-irradiated and irradiated PP/EG composites without SDS treatment exhibited a sharp transition from insulator to conductor, with a significant

lowering of the percolation threshold for the irradiated samples. Both non-irradiated and irradiated PP/SDS-EG showed little increase in electrical conductivity over the investigated EG content range, which was attributed to the SDS forming an isolation layer around the EG particles. The degradation temperatures at 50 % mass loss did not significantly change up to 6 wt% EG content for the non-irradiated samples containing EG and SDS-EG, but they significantly increased for the samples with higher filler contents. No trend could be observed for the irradiated samples, probably because of an inconsistent combination of crosslinking and degradation as a result of the irradiation. Both the addition of filler and irradiation gave rise to brittle samples. Increasing filler content generally gave rise to reduced tensile strength values, while irradiation did not significantly change these values. The tensile modulus values generally increased with increasing filler content, as a result of the higher modulus of the filler particles, and with irradiation, probably as a result of crosslinking.

References

1. Kalaitzidou K, Fukushima H, Drzal LT (2007) Mechanical properties and morphological characterization of exfoliated graphite-polypropylene nanocomposites. Composites A 38:1675–1682. doi:10.1016/j.compositesa.2007.02.003
2. Ranjbar M, Arefazar A, Bakhshandeh G (2013) Constituting balance between strength and toughness in nanocomposites based on PP/SEBS-g-MA blends. J Thermoplast Compos Mater 2:1–8. doi:10.1177/0892705712475001
3. Prashantha K, Lacrampe MF, Krawczak P (2011) Processing and characterization of halloysite nanotubes filled polypropylene nanocomposites based on a masterbatch route: effect of halloysites treatment on structural and mechanical properties. eXPRESS Polymer Lett 5:295–307. doi:10.3144/expresspolymlett.2011.30
4. Kalaitzidou K, Fukushima H, Askeland P, Drzal LT (2008) The nucleating effect of exfoliated graphite nanoplatelets and their influence on the crystal structure and electrical conductivity of polypropylene nanocomposites. J Mater Sci 43:2895–2907. doi:10.1007/s10853-007-1876-3
5. Prashantha K, Soulestin J, Lacrampe MF, Claes M, Dupin G, Krawczak P (2008) Multi-walled carbon nanotube filled polypropylene nanocomposites based on masterbatch route: Improvement of dispersion and mechanical properties through PP-g-MA addition. eXPRESS. Polymer Lett 2:735–745. doi:10.3144/expresspolymlett.2008.87
6. Kashiwagi T, Grulke E, Hilding J, Groth K, Harris R, Butler K, Shields J, Kharchenko S, Douglas J (2004) Thermal and flammability properties of polypropylene/carbon nanotube nanocomposites. Polymer 45:4227–4239. doi:10.1016/j.polymer.2004.03.088
7. Bikiaris D (2010) Microstructure and properties of polypropylene/carbon nanotube nanocomposites. Materials 3:2884–2946. doi:10.3390/ma3042884

8. Huegun A, Fernández M, Muñoz ME, Santamaría A (2012) Rheological properties and electrical conductivity of irradiated MWCNT/PP nanocomposites. Compos Sci Technol 72:1602–1607. doi:10.1016/j.compscitech.2012.06.011

9. Ma J, Deng H, Peijs T (2010) Processing of poly(propylene)/carbon nanotubes composites using scCO$_2$-assisted mixing. Macromol Mater Eng 295:566–574. doi:10.1002/mame.200900405

10. Afanasov IM, Savchenko DV, Ionov SG, Rusakov DA, Seleznev AN, Avdeev VV (2009) Thermal conductivity and mechanical properties of expanded graphite. Inorg Mater 45:486–490. doi:10.1134/S0020168509050057

11. Ramimoghadam D, Hussein MZB, Taufiq-Yap YH (2012) The effect of sodium dodecyl sulfate (SDS) and cetyltrimethylammonium bromide (CTAB) on the properties of ZnO synthesized by hydrothermal method. Int J Mol Sci 13:1327–13293. doi:10.3390/ijms131013275

12. Güngör N, Alemdar A, Atici O, Ece IO (2001) The effect of SDS surfactant on the flow and zeta potential of bentonite suspensions. Mater Lett 51:250–254

13. Costache MC, Heidecker M, Manias E, Gupta R, Wilkie C (2007) Benzimidazolium surfactants for modification of clays for use with styrenic polymers. Polymer Degrad Stab 92:1–23. doi:10.1016/j.polymdegradstab.2007.08.001

14. Lee K-Y, Kim K-Y (2008) ^{60}Co γ-ray irradiation effect and degradation behaviours of a carbon nanotubes and poly(ethylene-co-vinyl acetate) nanocomposites. Polymer Degrad Stab 93:1290–1299. doi:10.1016/j.polymdegrastab.2008.04.007

15. Martínez-Morlanes MJ, Castell P, Alonso PJ, Martinez MT, Puértolas JA (2012) Multi-walled carbon nanotubes acting as free radical scavengers in gamma-irradiated ultrahigh molecular weight polyethylene composites. Carbon 50:2442–2452. doi:10.1016/j.carbon.2012.01.066

16. Hwang TY, Lee S, Kang P-H, Park KH, Ahn Y, Lee JW (2011) The effect of electron beam irradiation on the dispersion and properties of poly(ethylene-co-vinyl acetate)/clay nanocomposites. Macromol Res 19:1151–1156. doi:10.1007/s13233-011-1104-5

17. Khodkar F, Ebrahimi NG (2011) Effect of irradiation on mechanical and structural properties of ethylene vinyl acetate copolymers hollow fibres. J Appl Polymer Sci 119:2085–2092. doi:10.1002/app.32926

18. Kalaitzidon K, Fukushima H, Drzal LT (2007) A new compounding method for exfoliated graphite-polypropylene nanocomposites with enhanced flexural properties lower percolation threshold. Compos Sci Technol 67:2045–2051. doi:10.1016/j.compscitech.2006.11.014

19. Kalaitzidon K, Fukushima H, Drzal LT (2007) A new compounding method for exfoliated graphite-polypropylene nanocomposites with enhanced flexural properties lower percolation threshold. Compos Sci Technol 67:2045–2051. doi:10.1016/j.compscitech.2006.11.014

20. Quan H, Zhang B-Q, Zhao Q, Yuen RKK, Li RKY (2009) Facile preparation and thermal degradation studies of graphite nanoplatelets (GNPs) filled thermoplastic polyurethane (TPU) nanocomposites. Composites A 40:1506–1513. doi:10.1016/j.compositesa.2009.06.012

21. Cheng S, Chen X, Hsuan YG, Li CY (2012) Reduced graphene oxide-induced polyethylene crystallization in solution and nanocomposites. Macromolecules 45:993–1000. doi:10.1021/ma201214531

22. Bose S, Kulia T, Uddin ME, Kim NH, Lau AKT, Lee JH (2010) In situ synthesis and characterization of electrically conductive polypyrrole/graphene nanocomposites. Polymer 51:5921–5928. doi:10.1016/j.polymer.2010.10.014

23. Yuan XY, Zou LL, Liao CC, Dai JW (2012) Improved properties of chemically modified graphene/poly(methyl methacrylate) nanocomposites via a facile in situ bulk polymerization. eXPRESS. Polymer Lett 6:847–858. doi:10.3144/expresspolymlett.2012.90

24. Wunderlich B (1990) Thermal analysis. Academic Press, New York

25. Galeski A (1999) Polypropylene: An A-Z reference series. Polymer science and technology series vol. 2, J. Karger-Kocsis (Ed.). ISBN: 978-94-011-4421-6

26. Causin V, Marega C, Marigo A, Ferrara G, Ferraro A (2006) Morphological and structural characterization of polypropylene/conductive graphite nanocomposites. Eur Polymer J 42:3153–3161. doi:10.1016/j.europolymj.2006.08.017

27. Wang Y, Tsai H-B (2012) Thermal, dynamic-mechanical and dielectric properties of surfactant intercalated graphite oxide filled maleated polypropylene nanocomposites. J Appl Polym Sci 123:3154–3163. doi:10.1002/app.34976

28. Zhang Y-Q, Lee J-H, Rhee JM, Rhee KY (2004) Polypropylene-clay nanocomposites prepared by in situ grafting-intercalating in melt. Compos Sci Technol 64:1383–1389. doi:10.1016/j.compscitech.2003.10.014

29. Piana F, Pionteck J (2013) Effect of the melt processing conditions on the conductive paths formation in thermoplastic polyurethane/expanded graphite (TPU/EG). Compos Sci Technol 80:39–46. doi:10.1016/j.compscitech.2013.03.002

30. S.V.J. Canevarolo (Ed.) (2003) Techniques for polymer characterization. Ed Artliber, São Paulo

31. Huo H, Jiang S, An L (2004) Influence of shear on crystallization behaviour of the β phase in isotactic polypropylene with β-nucleating agent. Macromolecules 37:2478–2483. doi:10.1021/ma0358531

32. Sefadi JS, Luyt AS, Pionteck J (2015) Effect of surfactant on EG dispersion in EVA and thermal and mechanical properties of the system. J Appl Polym Sci 132:41352. doi:10.1002/app.41352

33. Paul DR, Robeson LM (2008) Polymer nanotechnology: nanocomposites. Polymer 49:3187–3204. doi:10.1016/j.polymer.2008.04.017

34. Huang R, Xu X, Lee S, Zhang Y, Kim B-J, Wu Q (2013) High density polyethylene composites reinforced with hybrid inorganic fillers: morphology, mechanical and thermal expansion performance. Materials 6:4122–4138. doi:10.3390/ma6094122